A Varactor-Tuned Dual-Band Slot Antenna

Nader Behdad, *Student Member, IEEE,* and Kamal Sarabandi, *Fellow, IEEE*

***Abstract*—A new technique for designing dual-band reconfigurable slot antennas is introduced. The technique is based on loading a slot antenna with a lumped capacitor (or varactor) at a certain location along the slot. Given a fixed capacitor location along the slot, decreasing the capacitance results in increasing the first and second resonant frequencies of the slot antenna. However, the changes in the resonant frequencies are significantly different for the first and second resonances and, hence, a dual-band antenna with considerable frequency ratio tuning range can be obtained. Based on this technique, an electronically tunable dual-band antenna with a frequency ratio in the range of 1.2–1.65 is designed and fabricated using a single varactor with a capacitance range of 0.5–2.2 pF. The antenna has similar radiation patterns with low cross-polarization levels at both bands and across the entire tunable frequency range.**

***Index Terms*—Multifrequency antennas, multiple band antennas, reconfigurable antennas, slot antennas.**

I. Introduction

DUAL-band antennas are of interest in many wireless applications that use two different frequency bands for receiving and transmitting. Current advancements in printed antenna technology have resulted in a variety of different techniques for designing low profile, cost effective, and highly efficient dual-band antennas [1]. Most techniques make use of certain approaches to manipulate the current distribution at one of the higher order resonant modes of the structure to change its resonant frequency. For example, in [2], a rectangular patch antenna is loaded with a slot at a particular location such that it affects one resonant mode more than another, and this way a dual-band operation is obtained. However, the range of achievable frequency ratio (f_2/f_1) is limited to 1.6–2. This idea was later applied to circular and triangular patch antennas where frequency ratios of 1.3–1.4 and 1.35–1.5 were, respectively, achieved [3], [4]. Variations of these techniques with differently shaped slots and patches have also been investigated and discussed in detail in [1, Ch. 4].

The configuration and radiation characteristics of slot antennas appear to be more amenable to reconfigurability than their patch antenna counterparts. In a recent study, the design of a reconfigurable slot antenna was demonstrated with an octave band tunability using five PIN diode switches [5]. The drawback of this design, however, is that the PIN diodes are forward biased to change the resonant length of the antenna and significant amount of electric currents flows through each diode which, given the ohmic resistance associated with each diode, results in loss of RF power and, hence, reduces the antenna efficiency. In [6], a single-element dual-band CPW-fed slot antenna with similar radiation patterns at both bands is studied. However, this antenna shows high levels of cross-polarized radiation in its second band of operation. In [7], a compact dual-band CPW-fed slot antenna, with a size reduction of about 60% compared to a conventional slot antenna, is studied. However, this antenna is designed for two particular frequency bands, and little attention has been paid to investigating its frequency tuning capabilities. Furthermore, it suffers from high levels of cross-polarized radiation, which at some angles are equal or even larger than the copolarized component. Other topologies have also been used to achieve dual/multiband operations. Examples of these include structures that make use of parasitic elements and multiple radiating elements as described in [8] and [9]. Among other categories, design of a wideband/dualband relatively wide slot antenna fed by a microstrip line can be mentioned. It is shown that, for a rectangular slot with width to length ratios larger than 0.15, a dual-resonant behavior can be achieved and frequency ratios from 1.1 to 1.7 can easily be obtained by choosing the appropriate location for the feed [10]. The antenna is shown to have very small cross-polarization levels and similar radiation patterns at both bands.

In this paper, we propose a new technique for designing dual-band narrow slot antennas that can easily be modified to obtain a tunable antenna. Furthermore, the frequency ratio of the antenna will be determined by the applied dc bias voltage or by choosing the right value for the lumped element and not by changing the geometrical parameters of the antenna. The proposed technique is based on loading a slot antenna with a fixed or variable capacitor at a certain location along the slot. One of the advantages of this technique is that the current that flows through a capacitor, or a reverse biased varactor, is small compared to a PIN diode or a MEMS switch and hence, the finite Q of the device does not deteriorate the antenna efficiency. As will be shown, such an antenna exhibits a dual resonant behavior. In addition, placing a capacitor in parallel with the slot results in reduction of its resonant frequency. This occurs for both the first and second resonant modes. However, the decrease is not uniform and depends on the location of the capacitor along the slot. It will be shown that the location of the capacitor can be chosen to minimize the variations of one mode and, therefore, obtain a dual-band antenna with adequate control over its frequency ratio. In what follows we will first develop an approximate transmission line model as a design tool for determining the resonant frequencies of the slot antenna for a given value and location of the capacitor. Exact location of the capacitor can then be obtained using full wave analysis of the antenna. Then a tunable dual-band antenna is designed in which a varactor, with its proper biasing network, is used

Manuscript received August 26, 2004; revised February 24, 2005. This work was supported in part by the Engineering Research Centers program of the National Science Foundation under NSF Award Number EEC-9986866.

The authors are with The Radiation Laboratory, Department of Electrical Engineering and Computer Science, The University of Michigan, Ann Arbor, MI 48109 USA (e-mail: behdad@umich.edu).

Digital Object Identifier 10.1109/TAP.2005.863373

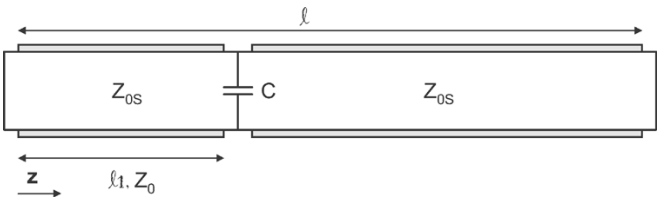

Fig. 1. Transmission line model of a slot antenna loaded with a lumped capacitor.

to tune the frequency ratio of the antenna. Finally, measured results for the radiation patterns and input reflection coefficients of the antenna are presented, compared with the simulation results, and discussed. It will be shown that the simulation and measurement results agree very well and the antenna has good simultaneous match at both bands with similar radiation patterns across the entire band of operation.

II. Loaded Slot Antennas for Dual-Band Operation

A resonant narrow slot antenna at its first resonance may be considered as a $\lambda/2$ transmission line, short circuited at both ends [11]. Loading such a structure with a capacitor as shown in Fig. 1, increases the line capacitance at one point and, therefore, reduces the frequency of its first and all higher order resonances. This reduction, however, is not uniform and depends on the location of the capacitor (ℓ_1 in Fig. 1), its value, and the slot line impedance. Applying the transverse resonance condition to the structure shown in Fig. 1 results in the following equation for the resonant frequencies of the structure

$$\tan(\beta(\omega)(\ell-\ell_1))+\tan(\beta(\omega)\ell_1) -\omega C Z_{0s}\tan(\beta(\omega)(\ell-\ell_1))\tan(\beta(\omega)\ell_1)=0 \quad (1)$$

where $\beta(\omega)$ is the frequency dependent, slot line propagation constant, C is the capacitance of the lumped capacitor, and ω is the angular frequency. This equation can be solved numerically as a function of frequency and capacitance value and for fixed values of ℓ_1 to obtain the resonant frequencies of the loaded slot. For different ℓ_1 values, this equation is solved for a loaded slot antenna with slot length and width of $\ell = 60$ mm and $w = 2$ mm, which is printed on a 0.5-mm-thick substrate with $\epsilon_r = 3.4$. The propagation constant $\beta(\omega)$ and impedance of this line, Z_{0s}, are calculated using equations provided in [12] and the results are shown in Fig. 2. The variations of f_1 and f_2 are seen to be dependent on ℓ_1 and C. However, this model does not take into account the effect of the antenna feed and its matching network, which affect the resonant frequencies of the antenna.

At its first resonance, the magnitude of the electric field of a slot antenna (and therefore the voltage magnitude) is maximum at the center of the slot and zero at the edges. On the other hand, the magnitude of the electric current that flows around the slot is minimum at the center and maximum at the edges [11]. Therefore, if the slot antenna is fed at the center, its input impedance, as seen from the feed terminals, will be very large (ratio of a large voltage to a small current). However, if the feed terminals move away from the center of the slot antenna and approach its edge, the observed input impedance drops until it assumes a value of zero when the feed terminals are right at the edge of the slot (and therefore are short circuited). Thus, it is possible to

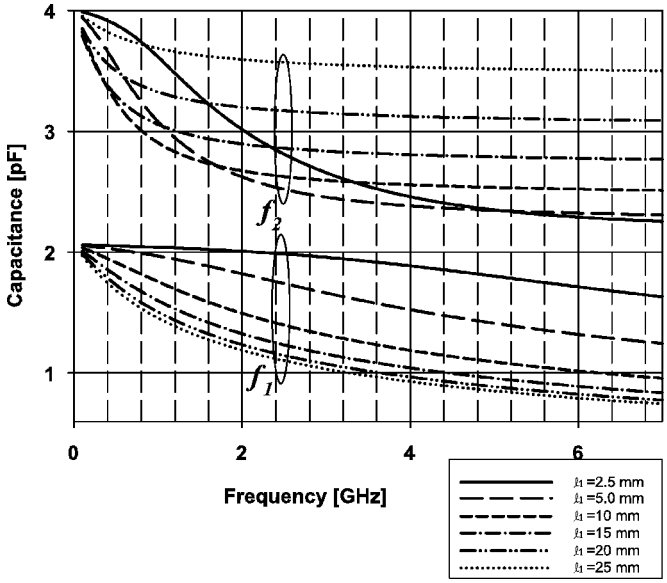

Fig. 2. First and second resonant frequencies of a loaded slot antenna (with $\ell = 60$ mm, $w = 2$ mm, $\epsilon_r = 3.4$, and the substrate thickness of 0.5 mm) as a function of value and location of the capacitor. The curves are obtained from solving (1) numerically.

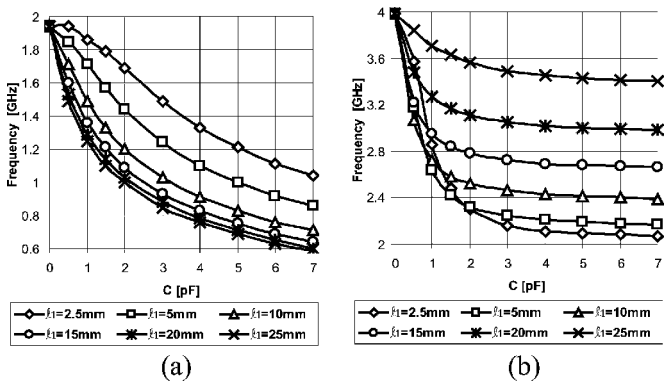

Fig. 3. Resonant frequencies of a microstrip-fed loaded slot antenna, with $\ell = 60$ mm and $w = 2$ mm printed on a substrate with $\epsilon_r = 3.4$ and thickness of 0.5 mm, obtained from full-wave simulations in IE3D. (a) First resonant frequency. (b) Second resonant frequency.

match the impedance of the antenna to a wide range of line impedances by choosing the right location for the feed (from center to the edge). In this paper, we use an open circuited, off-centered, microstrip line to feed the antenna. Therefore, in addition to choosing the feed location, the length of the open circuited microstrip line can be tuned such that it compensates the reactive part of the input impedance to obtain a good match. This way, the antenna can easily be matched to the line impedance by only choosing the appropriate location and length of the open circuited microstrip line (L_s and L_m as shown in Fig. 5). This feeding mechanism is very well known and is comprehensively studied in [11], [13], and [14] and in their references. Using full-wave simulations in IE3D [15], better approximations for the resonant frequencies of the first and second bands of the loaded slot antenna (for different values of ω, C, and ℓ_1) can be obtained. Fig. 3(a) and (b) shows the frequencies of the first and second resonances of a straight slot antenna with an overall length of $\ell = 60$ mm and a slot width of $w = 2$ mm, which

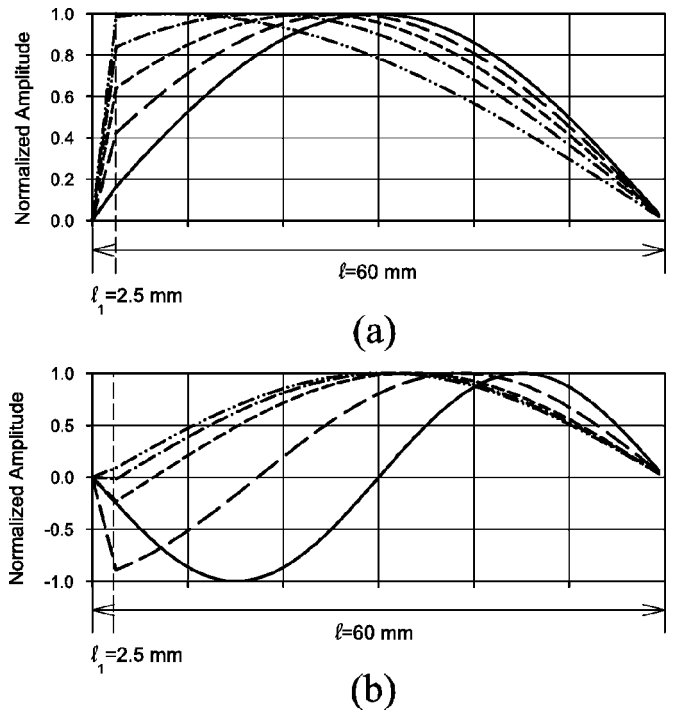

Fig. 4. Electric field distribution of a loaded slot antenna at (a) first and (b) second resonant frequencies. The antenna has $\ell = 60$ mm, $w = 2$ mm, $\ell_1 = 2.5$ mm, $\epsilon_r = 3.4$, and substrate thickness of 0.5 mm. Solid: C = 0 pF, Long-dashed: C = 1 pF, Short-dashed: C = 2 pF, Dash-dot: C = 3 pF, and Dash-dot-dot: C = 5 pF.

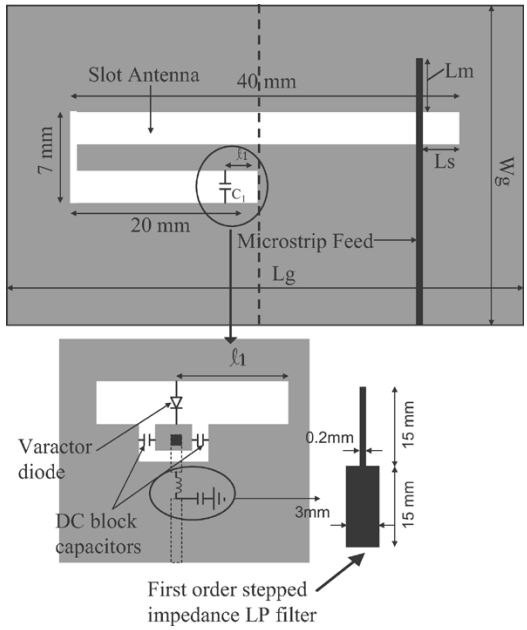

Fig. 5. Topology of the reconfigurable dual-band slot antenna of Section III.

is printed on a 0.5–mm-thick substrate with $\epsilon_r = 3.4$. This antenna is fed with a 50 Ω microstrip line with $L_s = 6$ mm and $L_m = 6$ mm. As can be seen from this figure, the first and second resonances of this antenna, without a capacitor, occur at 2 and 4 GHz, respectively. As C is increased, the frequencies of both of these resonances decrease. However, this decrease is a function of ℓ_1. For $\ell_1 = 2.5$ mm, and $0 \leq C \leq 2$ pF, the decrease in the frequency of the first resonance is much smaller than that of the second one [see Fig. 3(a) and (b)]. This suggests that a dual-band antenna, with a relatively constant f_1 and variable f_2 can be designed by only changing the value of C.

The radiation patterns of the antenna at the two bands are determined by the electric field distribution across the slot at the first and second resonances. The electric field distribution in the presence of the capacitor cannot easily be obtained from full-wave simulations. However, by using the equivalent model of Fig. 1, and solving the Maxwell's equations for the voltages and currents of the transmission line, in conjunction with the boundary conditions at $z = 0$, $z = \ell_1$, and $z = l$, the following expression for the normalized voltage (electric field) distribution across the transmission line (slot antenna) can be obtained

$$V(z) = \begin{cases} \frac{\sin(\beta(l-\ell_1))}{\sin(\beta\ell_1)} \sin(\beta z) & z \leq \ell_1 \\ \sin(\beta(l-z)) & z > \ell_1 \end{cases}. \qquad (2)$$

In this equation, the effect of the microstrip feed on the current distribution is ignored. However, examining it for different values of capacitance provides significant intuition in the operation of the antenna and its radiation patterns at both bands of operation. Fig. 4(a) and (b) shows the normalized electric field distribution across a straight slot antenna with $\ell = 60$ mm, $w = 2$ mm, and $\ell_1 = 2.5$ mm for different values of C. As can be seen in Fig. 4(b), the electric field distribution at the second resonance, when there is no capacitance, is antisymmetric and therefore the radiation pattern of this mode will have a null at broadside. This is significantly different from the radiation pattern of the first mode, which has maximum directivity at its broadside. In order to circumvent this problem and obtain a dual-band antenna with similar radiation patterns at both bands, the slot topology of Fig. 5 is used. In this case, the straight slot antenna is bent such that the longer (including the 7–mm bend) and shorter arms of the slot antenna are, respectively, $0.7\lambda_2$ and $0.3\lambda_2$ long at the second resonant frequency (λ_2 is the guided wavelength of the unloaded slot at the second resonant). The antenna shown in Fig. 5, still has the same model given in Fig. 1 and has the electric field distributions shown in Fig. 4(a) and (b). By bending the slot as shown in Fig. 5, the magnetic current at the lower section of the slot antenna is forced to flow in opposite direction relative to the current in the upper (longer) section of the slot antenna. If the length of the lower slot is at least $\lambda_2/4$ at the second resonant frequency, when the antenna is not loaded, these two oppositely directed currents have almost the same current distribution [as can be seen from Fig. 4(b)] with a 180° phase difference caused by bending the slot. Therefore, the part of the antenna to the left of the dashed line (see Fig. 5) does not significantly contribute to the far-field radiation of the second band. In this case, the radiation comes only from the part of the slot antenna to the right of the dashed line, which has an electric field distribution similar to that of the first mode. At the first resonance, however, the magnetic current of the lower part and upper part have different magnitudes; therefore, they do not completely cancel each other. Nevertheless, this somewhat reduces the radiation efficiency and can be viewed as a tradeoff for having consistent radiation patterns. In this case, the overall effective length of the lower slot is chosen to be slightly larger than $\lambda_2/4$. This length is optimized, using full wave simulations in IE3D, to ensure that the antenna will have similar radiation

TABLE I
PHYSICAL AND ELECTRICAL PARAMETERS OF THE DUAL-BAND RECONFIGURABLE SLOT ANTENNA

Parameter	L_g	W_g	L_s	L_m
Value	12 cm	10 cm	6 mm	6.0 mm
Parameter	f_2/f_1 range	RF/DC isolation	V_{DC}	Capacitance range
Value	1.2-1.65	Min. of 24 dB	1.5 V-30 V	0.5 pF-2.2 pF

patterns at both bands when the effects of the microstrip feed and the loading capacitors are considered. In the next section, simulation and measurement results of the antenna are presented and discussed.

III. SIMULATION, FABRICATION, AND MEASUREMENT OF THE RECONFIGURABLE DUAL-BAND ANTENNA

A. Simulation and Measurement Results

The bias network of the varactor used in tuning the antenna is shown in Fig. 5. The dc bias voltage is isolated from the RF by cutting the ground plane around the varactor cathode. The RF connectivity around the slot antenna is achieved using two large capacitors that connect the cathode path to the surrounding ground plane. The antenna is fed with an off-centered microstrip line, and the length of the open circuited line L_m and its position L_s are tuned to obtain good simultaneous match at both bands. The antenna is designed to operate on a 0.5-mm-thick RO4350B substrate with $\epsilon_r = 3.4$, $\tan\delta = 0.003$, and ground plane size of 12 *cm* × 10 *cm* (Table I). A high quality varactor manufactured by Metelics (SODT 3001) with a tuning range of 0.5 to 2.2 pF for $30\ \mathrm{V} \geq V_{\mathrm{dc}} \geq 0\ \mathrm{V}$ is used. In order to improve the dc/RF isolation, a first-order low-pass filter is placed in the path of the dc bias line. The filter is implemented using stepped impedance microstrip lines with a rejection band covering the frequency range of 1.5 to 4 GHz, which covers the entire band of operation of the antenna.

The antenna is then simulated using IE3D, which is a full-wave simulation tool based on the method of moments [15], and its input reflection coefficient and radiation patterns are studied for various different varactor values. The antenna is then fabricated on the same 12 cm × 10 cm, RO4350B substrate and its S_{11} spectral response is measured using a calibrated vector network analyzer. The simulated and measured S_{11} of this antenna, for different bias voltages, are presented in Fig. 6(a) and (b), respectively. The simulation results indicate that good simultaneous impedance match at both bands can be obtained by just choosing the appropriate values of L_s and L_m (Fig. 5). Fig. 6(b) shows that by increasing the dc bias voltage from 1.5 to 30 V, the frequency of the first resonance is increased from 1.8 to 1.95 GHz. However, this change is fast for small values of bias voltage and exhibits a saturation behavior for bias voltage values beyond 6 V. On the other hand the resonant frequency of the second band increases from 2.15 to 3.22 GHz in a rather smooth fashion. In order to compare the measurement and simulation results more easily, the simulated and measured values of the operating frequencies of the antenna are presented in Fig. 7 as a function of the applied dc bias voltage of the varactor. The maximum error between the predicted and measured values of the operating frequencies are

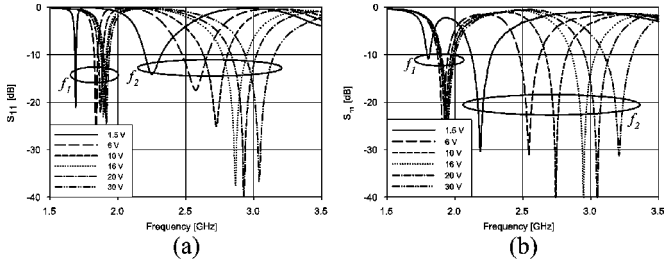

Fig. 6. S_{11} of the dual-band reconfigurable slot antenna of Section III for different bias voltages. (a) Simulation. (b) Measurement.

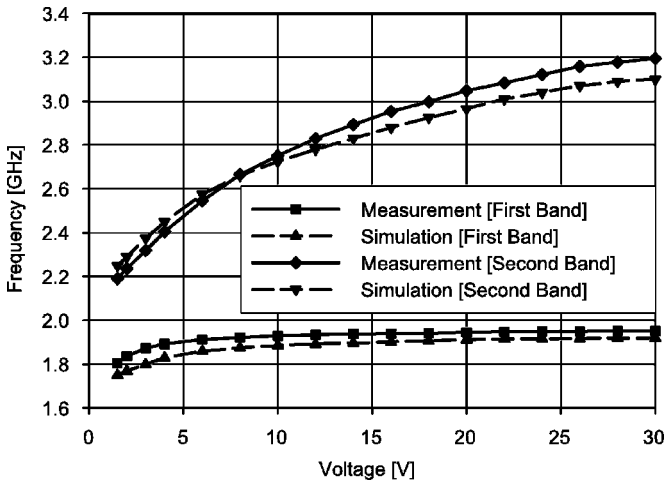

Fig. 7. Comparison between the measured and simulated operating frequencies of the first and second bands of the dual-band reconfigurable slot antenna of Section III.

3.6% and 3% for the first and second bands, respectively. The discrepancies between the two results can mostly be attributed to the inaccuracies in the fabrication process (alignment errors), uncertainties in the exact permittivity of the substrate ($\pm 3\%$ error specified by the manufacturer), uncertainties in the capacitance values of the varactor diode, and numerical errors in the simulation results. Nevertheless, a good agreement between the simulation and measurement (with a maximum error of 3.6%) is observed.

Fig. 8 shows the measured and simulated frequency ratios of the antenna as a function of the varactor's dc bias voltage. It is observed that by changing the bias voltage from 1.5 to 30 V the frequency ratio (f_2/f_1) can continuously be tuned from 1.2 to 1.65. For bias voltage values below 1.5 V, simultaneous matching at both bands cannot be easily obtained. However, for $V_{\mathrm{dc}} > 1.5$ V a very good simultaneous match is obtained only by choosing the length of the open circuited microstrip line, L_m, and its location, L_s, appropriately [11], [13], and [14]. The RF to dc isolation of the antenna is also measured using a VNA and

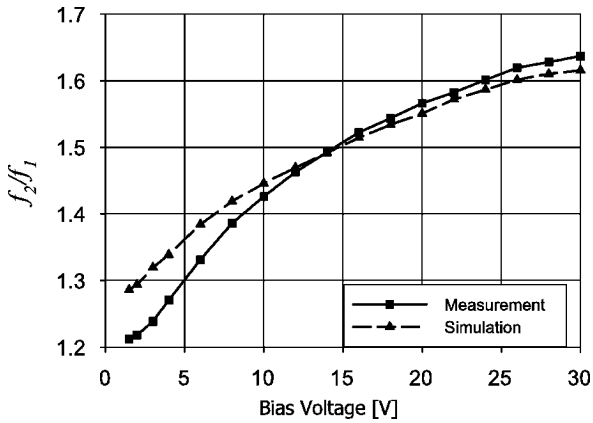

Fig. 8. Simulated and measured frequency ratio (f_2/f_1) of the reconfigurable slot antenna of Section III as a function of applied dc bias voltage.

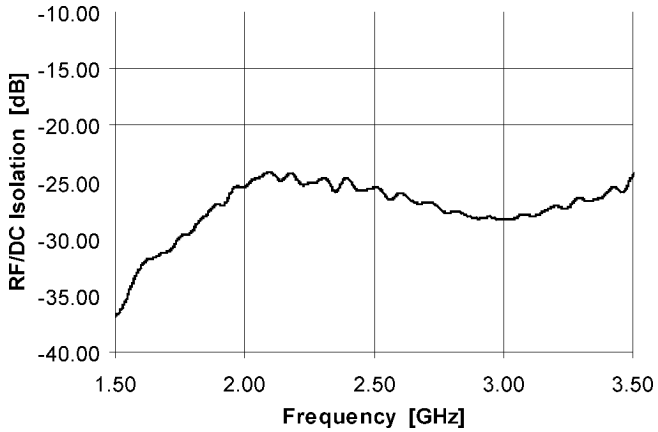

Fig. 9. Measured RF to dc isolation of the dual-band reconfigurable slot antenna of Section III.

is shown in Fig. 9. The RF to dc port isolation of better than 24 dB across the entire band of operation is demonstrated.

The radiation patterns of the antenna, for bias voltages of $V_{\rm dc} = 4$ V, 10, 20, and 30 V, are simulated in IE3D and the simulated patterns in the E and H planes are presented in Figs. 10–12, respectively. The radiation patterns of the antenna, for the same dc bias voltages, are also measured in the anechoic chamber of the University of Michigan and are presented in Figs. 11–13. Since the antenna is bidirectional and is almost symmetric with respect to the plane containing it, the fields in the lower half-space are similar to those in the upper half-space. Therefore, only the pattern plots in the range of $0° < \theta < 90°$ are shown.

Fig. 10(a) and (b) shows the simulated co- and cross-polarized radiation patterns of the antenna in E-plane for the first and second bands, respectively. It is observed that the antenna has similar radiation patterns at both bands and the shape of the pattern in this plane does not strongly depend on the applied bias voltage. Fig. 11(a) and (b) shows the measured co- and cross-polarized radiation patterns of the antenna in the E-plane for the first and second bands, respectively. The measurement results also indicate that the antenna has similar patterns at both bands. Furthermore, low levels of cross-polarized radiation are observed. The cross-polarization levels are, however, larger in

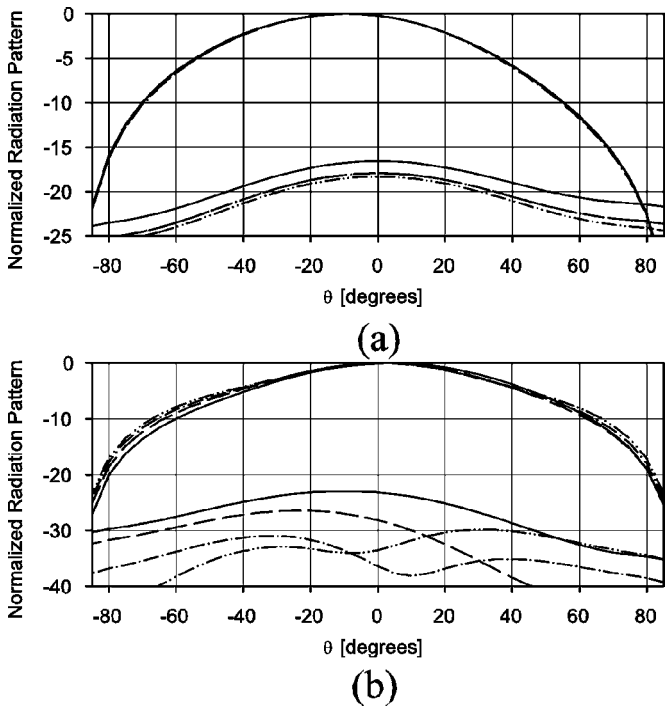

Fig. 10. Simulation results for the E-plane co- and cross-polarized radiation patterns of the dual-band slot antenna of Section III at (a) first band and (b) second band. Solid line: $V_{\rm dc} = 4$ V, Dash-dash: $V_{\rm dc} = 10$ V, Dash-dot: $V_{\rm dc} = 20$ V, and Dash-dot-dot: $V_{\rm dc} = 30$ V.

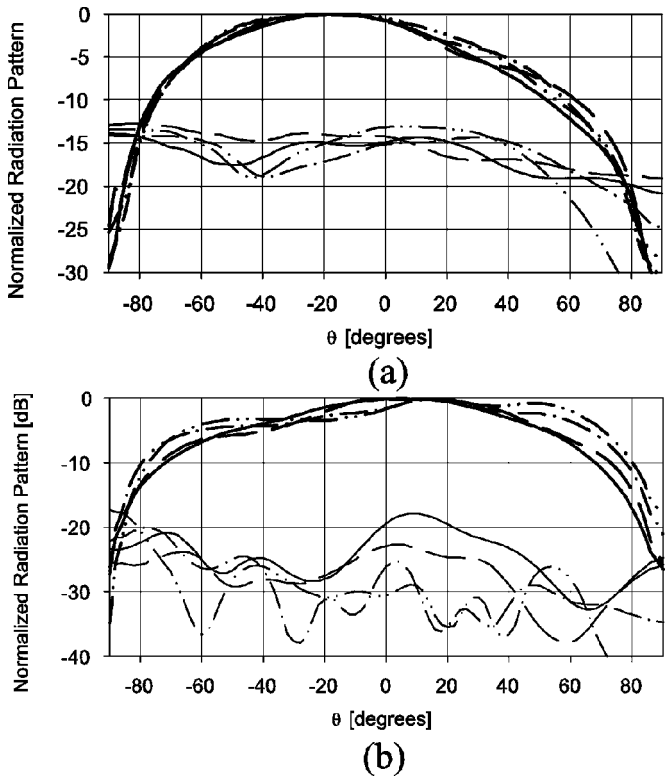

Fig. 11. Measured E-plane co- and cross-polarized radiation patterns of the dual-band slot antenna of Section III at (a) first band and (b) second band. Solid line: $V_{\rm dc} = 4$ V, Dash-dash: $V_{\rm dc} = 10$ V, Dash-dot: $V_{\rm dc} = 20$ V, and Dash-dot-dot: $V_{\rm dc} = 30$ V.

the first band due to the larger values of the electric field magnitude at the bent section. The simulated and measured radiation

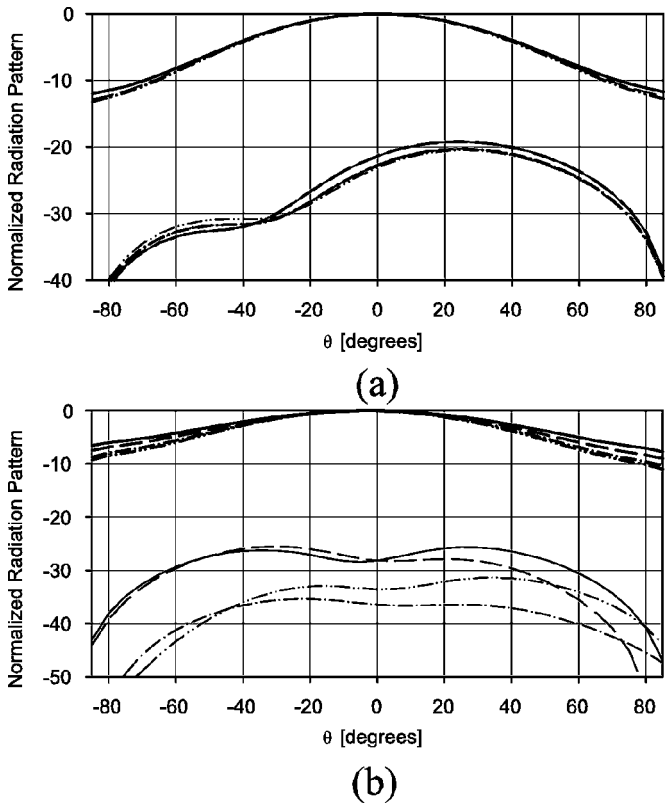

Fig. 12. Simulated H-plane co- and cross-polarized radiation patterns of the dual-band slot antenna of Section III at (a) first band and (b) second band. Solid line: $V_{\rm dc} = 4$ V, Dash-dash: $V_{\rm dc} = 10$ V, Dash-dot: $V_{\rm dc} = 20$ V, and Dash-dot-dot: $V_{\rm dc} = 30$ V.

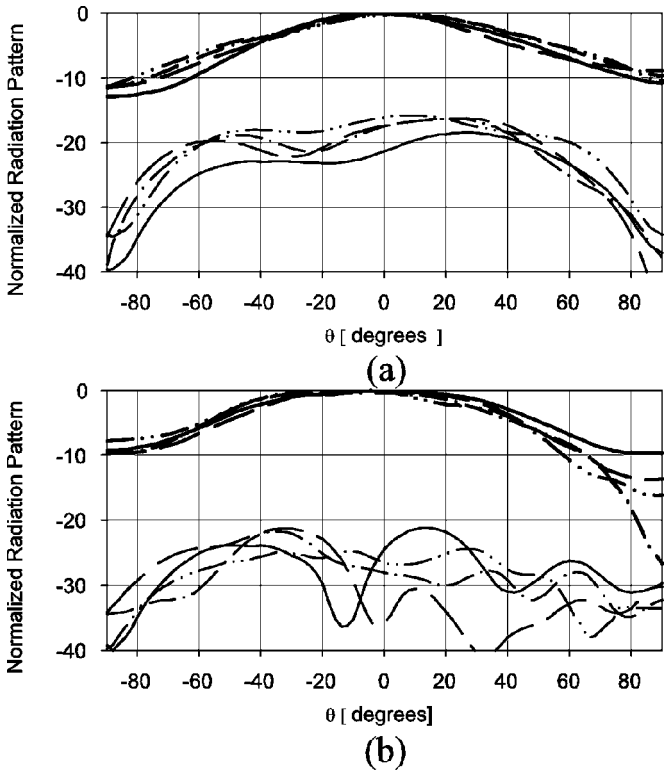

Fig. 13. Measured H-plane co- and cross-polarized radiation patterns of the dual-band slot antenna of Section III at (a) first band and (b) second band. Solid line: $V_{\rm dc} = 4$ V, Dash-dash: $V_{\rm dc} = 10$ V, Dash-dot: $V_{\rm dc} = 20$ V, and Dash-dot-dot: $V_{\rm dc} = 30$ V.

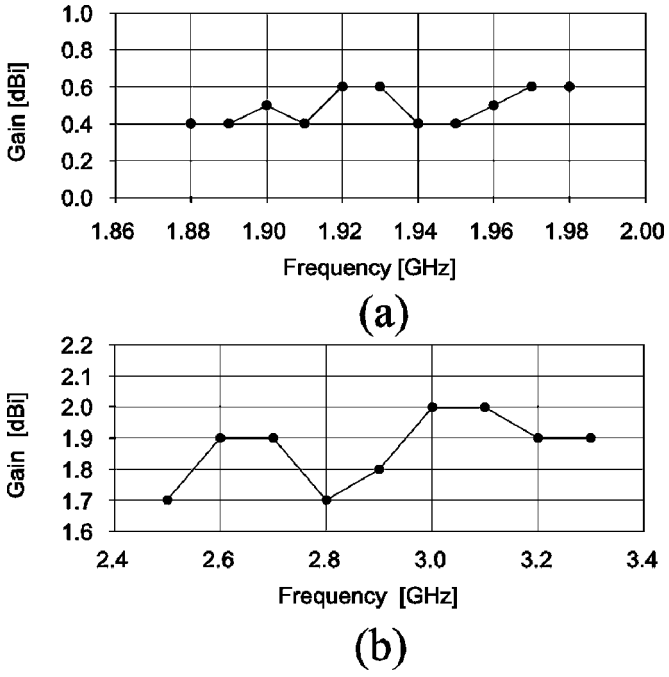

Fig. 14. Measured gain of the dual-band reconfigurable slot antenna of Section III. (a) First band. (b) Second band.

patterns in the H-plane are presented in Figs. 12 and 13, respectively. Fig. 12(a) and (b) shows the simulated H-plane pattern of the antenna at the two bands for different bias voltage values where as before similar radiation patterns at both bands and for different bias voltage values are observed. Fig. 13(a) and (b) shows the measured H-plane radiation patterns of the antenna for the first and second bands. It is observed that the radiation patterns of the antenna, in the H-plane, are also similar to each other for both frequency bands and for different bias voltages. Comparison of the simulated radiation patterns of Figs. 10–12 with the measured radiation patterns of Figs. 11–13 shows that the copolarized simulated and measured radiation patterns are in a relatively good agreement with each other whereas the cross-polarized components are not. The discrepancies between the simulation and measurement radiation patterns can be attributed to the presence of the coaxial cables and connectors, which feed the antenna and bias the varactor diode, in close proximity to the antenna during the pattern measurements. The induced currents on these components radiate and distort both the copolarized and the cross-polarized components of the radiation patterns of the antenna. Since the cross-polarized component generated by the antenna is much weaker than its copolarized component, the distortions caused by the cables and connectors completely change the shape of the cross-pol pattern but only moderately affect the co-pol component.

The gain of the antenna is also measured across the entire band of operation using a double-ridged horn as a reference and is shown in Fig. 14. The antenna shows an average 0.5 dB gain at the first band and 1.8 dB at the second band of operation in the direction of maximum radiation. The lower gain of the first band is a result of smaller electrical dimensions of the antenna at this band. The lower bound of the efficiency of the antenna can be calculated using the measured gain values of the loaded antenna

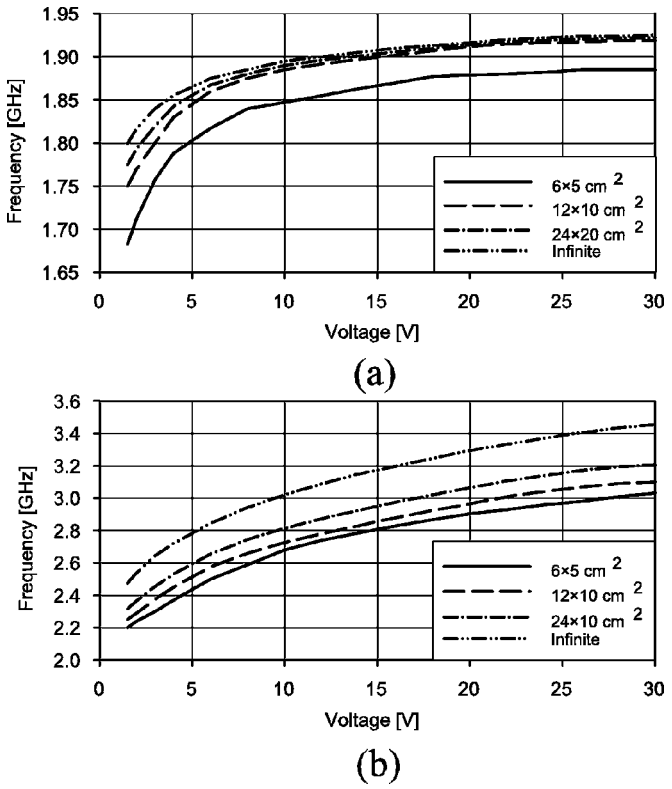

Fig. 15. Simulated results of the operating frequencies of the dual-band reconfigurable slot antenna, shown in Fig. 5, as a function of the varactor bias voltage for different ground plane sizes. (a) First band. (b) Second band.

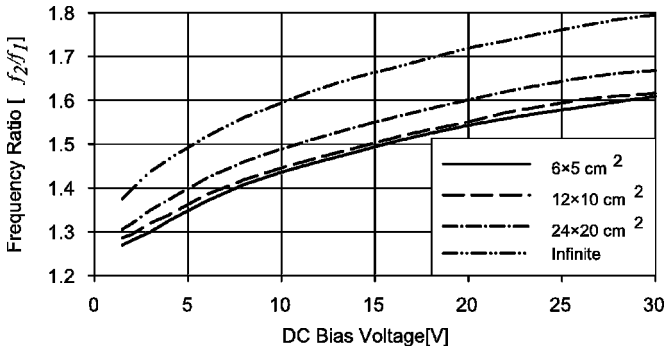

Fig. 16. Simulated results of the frequency ratios (f_2/f_1) of the dual-band reconfigurable slot antenna, shown in Fig. 5, as a function of the varactor bias voltage for different ground plane sizes.

and simulated directivity values for an unloaded antenna. Based on this calculation, the lower bound efficiency of 70% and 85% for the first and second bands are calculated. The major factor that contributes to the reduced efficiency of the antenna is its topology and the reduction of its electrical size that occurs as a result of capacitive loading [16]. Nevertheless, as these lower bound values indicate, the antenna radiates rather efficiently.

B. Finite Ground Plane Effects

The dimensions of the ground plane of a slot antenna affect its electrical and radiation parameters such as the radiation pattern, resonant frequency, and the gain of the antenna. For a single band slot antenna, these effects have extensively been studied in [17]–[23]. The effects of the finite ground plane size on the radiation patterns of a slot antenna are examined in [17] and [18]. In [17], the edge diffractions of surface waves in a slot antenna are modeled and it is shown that these diffractions cause ripples in the radiation patterns. In [19], the effects of finite ground plane size on bandwidth and gain of a U-shaped slot antenna are studied. The effects of the finite ground plane on the input matching and radiation parameters of a microstrip-fed cavity backed slot antenna are examined in [23]. In [20], [21], and [22], the effects of the ground plane dimensions on the gain and bandwidth of electrically small slot antennas are examined. It is shown that as the ground plane dimensions are increased, the antenna gain increases and approaches the gain of the antenna with an infinitely large ground plane size.

Since the effects of finite ground plane size on the radiation patterns and the gain of slot antennas are well known, in this paper we only examine the effects of the finite ground plane size on the resonant frequencies and frequency ratios of the dual-band reconfigurable slot antenna of Section III. In order to do this, full-wave simulations have been performed on the antenna shown in Fig. 5 for four different ground plane sizes of 6 cm $\times$ 5 cm, 12 cm $\times$ 10 cm, 24 cm $\times$ 20 cm, and ∞. Fig. 15(a) and (b) shows the effect of the ground plane size on the frequencies of the first and second bands of the dual-band antenna. As is observed from this figure, for fixed antenna and feed network dimensions, the resonant frequencies of both the first and second bands increase as the ground plane size increases and approach the resonant frequencies of the antenna with an infinitely large ground plane. Fig. 16 shows the effect of the ground plane size on the frequency ratio of the second band to that of the first band for the tunable antenna. Similar to the previous case, for fixed antenna dimensions and bias voltage, the frequency ratio increases as the ground plane size increases. As can be observed from Figs. 15 and 16, the ground plane size moderately affects the frequency response of the antenna. However, these effects can be taken into account in the simulation process and a very good agreement between the measurement and simulation results can be obtained as shown in Section III-A.

IV. Conclusion

A new technique for designing dual-band reconfigurable slot antennas is proposed. The technique is successfully applied to design a dual-band slot antenna with similar radiation patterns at both bands. Measurement results of the antenna indicate that it has a frequency ratio (f_2/f_1) that continuously increases from 1.2 to 1.65 by increasing its dc bias voltage from 1.5 to 30 V. Furthermore, good simultaneous matching is observed at both bands for the entire range of bias voltages, low levels of cross-polarized radiation is observed, and the radiation patterns of each band remain practically unchanged as the dc bias voltage is changed.

References

[1] K. L. Wong, *Compact and Broadband Microstrip Antennas*. New York: Wiley, 2002.

[2] S. Maci, B. B. Gentili, P. Piazzesi, and C. Salvador, "Dual band slot-loaded patch antenna," *Proc. Inst. Elect. Eng. Microw. Antennas Propag.*, vol. 142, no. 3, pp. 225–232, Jun. 1995.

[3] K. B. Hsieh and K. Wong, "Inset microstrip-line-fed dual-frequency circular microstrip antenna and its application to a two-element dual-frequency microstrip array," *Proc. Inst. Elect. Eng. Microw. Antennas Propag.*, vol. 147, pp. 359–361, Oct. 1999.
[4] S. T. Fang and K. L. Wong, "A dual frequency equilateral triangular microstrip antenna with a pair of two narrow slots," *Microw. Opt. Technol. Lett.*, vol. 23, pp. 82–84, Oct. 1999.
[5] D. Peroulis, K. Sarabandi, and L. P. B. Katehi, "A planar VHF reconfigurable antenna," in *Proc. IEEE Antennas and Propagation Society Int. Symp.*, vol. 1, Boston, MA, Jul. 2001, pp. 154–157.
[6] D. Llorens, P. Otero, and C. C. Penalosa, "Dual-band, single CPW port, planar slot antenna," *IEEE Trans. Antennas Propag.*, vol. 51, pp. 137–139, Jan. 2003.
[7] C. Wang, J. Lee, and R. Huang, "Experimental studies of a miniaturized CPW-fed slot antenna with the dual-frequency operation," *IEEE Antennas Wireless Propag. Lett.*, vol. 2, pp. 151–154, 2003.
[8] T. Morioka, S. Araki, and K. Hirasawa, "Slot antenna with parasitic element for dual band operation," *Electron. Lett.*, vol. 33, pp. 2093–20 944, Dec. 1997.
[9] J. S. Chen, "Triple-frequency annular-ring slot antennas fed by CPW and microstrip line," in *Proc. IEEE APS/URSI Int. Symp.*, vol. 2, Columbus, OH, Jun. 22–27, 2003, pp. 557–560.
[10] N. Behdad and K. Sarabandi, "A wide-band slot antenna design employing a fictitious short circuit concept," *IEEE Trans. Antennas Propag.*, vol. 53, pp. 475–482, Jan. 2005.
[11] Garg *et al.*, *Microstrip Antenna Design Handbook*. Norwood, MA: Artech House, 2001, ch. 7.
[12] Gupta *et al.*, *Microstrip Lines and Slotlines*, 2nd ed: Artech House, 1996.
[13] B. Das and K. Joshi, "Impedance of a radiating slot in the ground plane of a microstripline," *IEEE Trans. Antennas Propag.*, vol. 30, pp. 922–926, Sep. 1982.
[14] J. P. Kim and W. S. Park, "Network modeling of an inclined and off-center microstrip-fed slot antenna," *IEEE Trans. Antennas Propag.*, vol. 46, pp. 1182–1188, Aug. 1998.
[15] *IE3D*, Zeland Software Co..
[16] L. J. Chu, "Physical limitations on omni-directional antennas," *J. Appl. Phys.*, vol. 19, pp. 1163–1175, Dec. 1948.
[17] B. Stockbroeckx, I. Huynen, and A. V. Vorst, "Effect of surface wave diffraction on radiation pattern of slot antennaetched in finite ground plane," *Electron. Lett.*, vol. 36, pp. 1444–1446, Aug. 2000.
[18] R. M. DeFelice Souza, F. DaCosta Silva, and A. J. Giarola, "Effect of a finite ground plane thickness on the radiation pattern of an aperture antenna," in *Proc. IEEE Antennas and Propagation Society Int. Symp.*, vol. 1, Syracuse, NY, Jun. 6–10, 1988, pp. 34–37.
[19] V. Natarajan, E. Chettiar, and D. Chatterjee, "Effect of ground plane size on the performance of a class of microstrip antennas on microwave substrates," in *Proc. IEEE Antennas and Propagation Society Int. Symp.*, vol. 4, Monterey, CA, Jun. 2004, pp. 4491–4494.
[20] K. Sarabandi and R. Azadegan, "Design of an efficient miniaturized UHF planar antenna," *IEEE Trans. Antennas Propag.*, vol. 51, pp. 1270–1276, Jun. 2003.
[21] R. Azadegan and K. Sarabandi, "A novel approach for miniaturization of slot antennas," *IEEE Trans. Antennas Propag.*, vol. 51, pp. 421–429, Mar. 2003.
[22] N. Behdad and K. Sarabandi, "Bandwidth enhancement and further size reduction of a class of miniaturized slot antennas," *IEEE Trans. Antennas Propag.*, vol. 52, pp. 1928–1935, Aug. 2004.
[23] B. Zheng and Z. Shen, "Effect of a finite ground plane on microstrip-fed cavity-backed slot antennas," *IEEE Trans. Antennas Propag.*, vol. 53, pp. 862–865, Feb. 2005.

Nader Behdad (S'98) was born in Mashhad, Iran, in 1977. He received the Bachelor of Science degree in electrical engineering from Sharif University of Technology, Tehran, Iran, in September 2000 and the Master of Science degree in electrical engineering from the University of Michigan, Ann Arbor, in 2003. He is currently working toward the Ph.D. degree in the Department of Electrical Engineering and Computer Science, University of Michigan.

From 2000 to 2001, he worked as a Design Engineer for the Electronics Research Center, Sharif University of Technology. Since January 2002, he has been working as a Research Assistant at the Center for Wireless Integrated Micro-Systems, University of Michigan.

Mr. Behdad is the recipient of the Best Student Paper Award in the Antenna Applications Symposium held in Monticelo, IL, in September 2003, winner of the second prize in the student paper competition of the USNC/URSI National Radio Science Meeting, Boulder, CO, in January 2004, and the recipient of the Horace H. Rackham Predoctoral Fellowship from the Rackham School of Graduate Studies, University of Michigan in 2005.

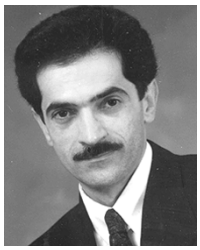

Kamal Sarabandi (S'87–M'90–SM'92–F'00) received the B.S. degree in electrical engineering from Sharif University of Technology, Tehran, Iran, in 1980, the M.S. degree in electrical engineering/mathematics, and the Ph.D. degree in electrical engineering from The University of Michigan-Ann Arbor, in 1986 and 1989, respectively.

He is the Director of the Radiation Laboratory and a professor with the Department of Electrical Engineering and Computer Science, University of Michigan. His research areas of interest include microwave and millimeter-wave radar remote sensing, electromagnetic wave propagation, and antenna miniaturization. He has 20 years of experience with wave propagation in random media, communication channel modeling, microwave sensors, and radar systems, and is leading a large research group including two research scientists, 10 Ph.D., and two M.S. students. Over the past 10 years, he has graduated 21 Ph.D. students. He has served as the Principal Investigator on many projects sponsored by NASA, JPL, ARO, ONR, ARL, NSF, DARPA, and numerous industries. He has published many book chapters and more than 120 papers in refereed journals on electromagnetic scattering, random media modeling, wave propagation, antennas, meta-materials, microwave measurement techniques, radar calibration, inverse scattering problems, and microwave sensors. He has also had more than 270 papers and invited presentations in many national and international conferences and symposia on similar subjects.

Dr. Sarabandi is a vice president of the IEEE Geoscience and Remote Sensing Society (GRSS), and a member of IEEE Technical Activities Board Awards Committee. He is serving as the Associate Editor of the IEEE TRANSACTIONS ON ANTENNAS AND PROPAGATION and the IEEE SENSORS JOURNAL. He is also a member of Commissions F and D of URSI and of The Electromagnetic Academy. He is listed in *American Men and Women of Science Who's Who in America* and *Who's Who in Science and Engineering*. He was the recipient of the Henry Russel Award from the Regent of The University of Michigan (the highest honor the University of Michigan bestows on a faculty member at the assistant or associate level). In 1999, he received a GAAC Distinguished Lecturer Award from the German Federal Ministry for Education, Science, and Technology given to about 10 individuals worldwide in all areas of engineering, science, medicine, and law. He was also a recipient of a 1996 EECS Department Teaching Excellence Award and a 2004 College of Engineering Research Excellence Award. In 2005, he received two prestigious awards, namely, the IEEE Geoscience and Remote Sensing Distinguished Achievement Award and the University of Michigan Faculty Recognition Award. In the past several years, joint papers presented by his students at a number of international symposia (IEEE AP'95,'97,'00,'01,'03, IEEE IGARSS'99,'02, IEEE IMS'01, URSI' 04,'05) have received top student prize paper awards.